

High- β plasma formation and observation of peaked density profile in RT-1

H. Saitoh, Z. Yoshida, J. Morikawa, Y. Yano, T. Mizushima,
Y. Ogawa, M. Furukawa, Y. Kawai, K. Harima, Y. Kawazura,
Y. Kaneko, K. Tadachi, S. Emoto, M. Kobayashi, T. Sugiura and
G. Vogel

Graduate School of Frontier Sciences, University of Tokyo, 5-1-5 Kashiwanoha, Kashiwa,
Chiba, Japan

Received 28 December 2010, accepted for publication 19 April 2011

Published 20 May 2011

Online at stacks.iop.org/NF/51/063034

Abstract

High- β ECH plasma is generated and stably sustained in a magnetospheric configuration, the Ring Trap 1 (RT-1) device, generated by a levitated dipole field magnet. Geomagnetic-field compensation and optimized operation have realized drastic improvements in plasma properties. The maximum local β value has reached 70% and the pressure profiles have a rather steep gradient near the superconducting magnet. Electrons of the high- β plasma typically consist of 70% hot (~ 50 keV) and the rest of cold populations. Confinement time of the hot component plasma is 0.5 s with the optimized neutral gas pressure. By removing the coil support structure, the peaked density profile is observed in the strong field region.

(Some figures in this article are in colour only in the electronic version)

1. Introduction

The Ring Trap 1 (RT-1) experiment is a magnetospheric configuration constructed for the confinement of ultra-high- β plasma which aims to enable advanced fusion using D–D and D– 3 He fuels [1, 2]. Dipole field is one of the most fundamental magnetic configurations in the Universe, and the goal of RT-1 is to realize high performance plasma confinement in the artificial magnetosphere. In the magnetospheric configuration, plasma is confined in a dipole field generated by a levitated superconducting magnet [3, 4], where the effects of flow and strongly inhomogeneous field play important roles in the confinement and stability properties of the plasma. The high- β confinement concept realized by the effects of the compressibility of flux tubes was first motivated by spacecraft observations in the Jovian magnetosphere [5]. Recently, the mechanism of high- β equilibrium has been theoretically explained by the hydrodynamic pressure of fast flow (double Beltrami state) [6–8]. Study of high- β flowing plasma is important for understanding the fundamental physics of the self-organization of magnetized charged particles, as well as for the realization of an advanced fusion concept. In high-temperature low-density plasma realized in RT-1 ($n_e \sim 10^{17} \text{ m}^{-3}$, $T_e \lesssim 50$ keV), the ion inertial length is comparable to or longer than the plasma scale length. Then a diversity of plasma structures can emerge by two-fluid effects due to the decoupling of ion and electron fluids [9].

RT-1 succeeded in generating its first plasma in 2006, and in the first series of experiments, plasma is generated and

sustained by electron cyclotron resonance heating (ECH) with 8.2 and 2.45 GHz microwaves [10–14]. Although ions are not heated and remain cold at present, we can investigate the properties of high- β plasma in a magnetospheric configuration using hot-electron plasma generated by ECH. In this study, we report the experimental results of the improved high- β ECH plasma in RT-1 realized by the optimization of plasma formation operation and compensation of the geomagnetic field [15]. The maximum local β value has reached 70%, and particle confinement time is approximately 0.5 s in the most recent experiment in RT-1. We found that the plasma pressure peak is located in the strong field region, and the electron density has peaked profiles near the superconducting magnet. Extensive studies have been carried out on the inward transport properties of plasma. Hasegawa [1] predicted radial inward diffusion of plasma that flattens density per flux tube, caused by the violation of the canonical angular momentum due to fluctuating fields. Observation of the peaked density profiles in high- β ECH plasma in RT-1 is consistent with the particle diffusion into the strong field region caused by the breaking of the third adiabatic invariant. Turbulent inward transport was reported in a dipole field configuration by LDX [4], and particle pinch effects were demonstrated by a gyrokinetic simulation [16]. Existence of particle pinch, caused by neoclassical and anomalous transport effects, was theoretically and experimentally confirmed in tokamaks [17], suggesting that transport towards the high-density region is one of the fundamental properties of plasma.

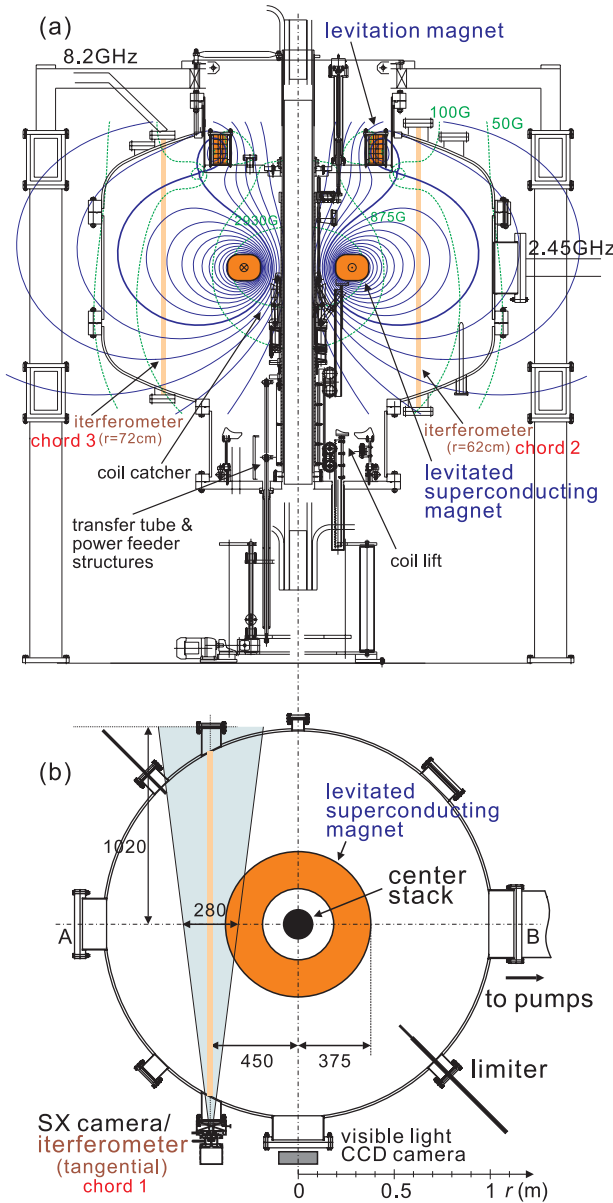


Figure 1. (a) Poloidal cross section and (b) top view of RT-1 including vacuum chamber, levitated and levitation coil magnets, magnet operation system, 2.45 and 8.2 GHz microwave waveguides and diagnostic system.

2. Experimental setup and recent progress

Figure 1 shows the cross sections of RT-1. Inside the chamber, RT-1 has a dipole field magnet made with Bi-2223 high-temperature superconducting wires, which generates a magnetosheric dipole field. In order to minimize perturbations to the plasma, the superconducting magnet of RT-1 is operated with a permanent current mode and magnetically levitated by a feedback-controlled normal-conducting levitation electromagnet located at the top of the chamber [12, 14]. The superconducting and levitation coils are operated with 250 and 28.8 kA, respectively. The combination of two magnets generates a separatrix configuration as shown in figure 1(a), and the plasma is separated from the chamber wall in the vacuum field. The dipole field coil is cooled

down to 20 K using three GM refrigerators, and we conduct 6 h of plasma experiment before the coil temperature rises to 30 K. In order to improve the accuracy of geomagnetic-field compensation, correction coils were replaced with a new system in 2008 [15]. The available microwave powers are 25 kW (1 s) at 8.2 GHz and 20 kW (2 s) at 2.45 GHz at present. The working gases are hydrogen and helium, which are continuously introduced into the vacuum chamber through a piezo-valve located at the bottom of the chamber. Detailed descriptions on the RT-1 device are presented in [13].

The diagnostic system of RT-1 is as follows: plasma diamagnetism is measured by four magnetic loops wound outside the chamber and multi-channel Hall probes installed inside the chamber. Equilibrium pressure profiles are estimated using Grad–Shafranov numerical analysis based on the magnetic measurements. According to the numerical analysis, we found an empirical relation between the averaged diamagnetic signal $\Delta\Psi$ and the maximum local β : $\beta(\%) \sim 18 \times \Delta\Psi$ (mWb) in the present plasma pressure range. The calculated β values also depend on the shapes of the pressure profiles. The above relationship gives a conservative value of the peak β for a given diamagnetic signal, avoiding the overestimation of the plasma pressure. A detailed description of the Grad–Shafranov analysis in RT-1 will be presented elsewhere. A 75 GHz (4 mm) microwave interferometer is used to measure the line-integrated electron density. Transmitting and receiving antennas of the interferometer were positioned at vertical ports at $r = 62$ or 72 cm (figure 1(a)) or tangential ports at $y = 45$ cm (figure 1(b)). We compared the interferometer data for similar conditions in different experiments, and estimated the density profiles of the plasma. For relatively low- β plasma generated by moderate microwave power, we also used edge Langmuir probes for the measurements of electron density and temperature profiles. For the measurements of bremsstrahlung x-ray energy distribution, Si(Li) detectors and pulse height analysis (PHA) systems were used in order to determine the hot-electron temperature and line-integrated density. An x-ray pinhole camera [18] with a 1024×1024 pixel 16 bit dynamic range CCD was used for imaging x-ray intensity (figure 1(b)). The x-ray camera can be used for the measurement of electron temperature by photon counting mode. Plasma fluctuations are measured by diamagnetic pickup coils, Langmuir probes and the interferometer. The magnetic pickup coil was located inside the chamber at $r = 92$ cm on the equator ($z = 0$ cm) plane, and used for the measurement of fluctuations up to ~ 10 MHz.

3. Improved high- β stable state

Plasma in the high- β and high-density state is generated depending on the filled neutral gas pressure P_n and injected microwave power P_f . Figure 2 shows diamagnetism $\Delta\Psi$ and line-averaged density n_e at various P_n and P_f at 2.45 GHz from 0.5 to 20 kW. $\Delta\Psi$ is an averaged signal of four magnetic loops, and n_e is inferred from measurements of the interferometer located at the tangential port. The maximum local β values of the plasma estimated from Grad–Shafranov numerical calculation is also shown in figure 2(a). The parameter ranges are designated as high-density, high- β and unstable modes

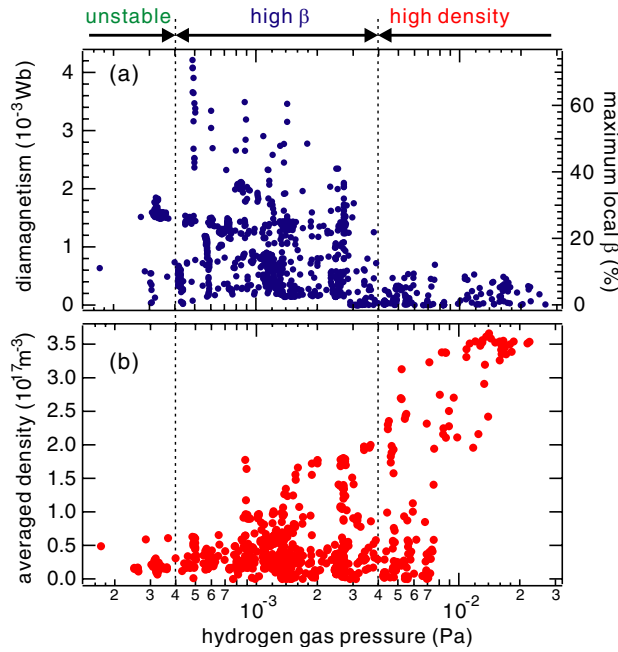


Figure 2. (a) Diamagnetic loop signal (averaged value of four loops and estimated maximum local β) and (b) line-averaged electron density, in the variation of neutral gas pressure.

depending on P_n as shown in the figure. The highest electron density is realized at $4 \text{ mPa} < P_n$, but the plasma has relatively low- β in this pressure range. High- β plasma is realized in the pressure range $0.4\text{--}4 \text{ mPa}$, which is characterized by large stored energy, strong x-ray radiation and depression of visible light strength and fluctuation levels. When P_n is lower than approximately 0.4 mPa , the plasma is unstable as described in the following sections, and it has rather low diamagnetic pressure and number density. In ECH experiments in RT-1 carried out so far, plasma pressure is mainly due to hot electrons. Thus the highest β was realized by increasing the input microwave power and lowering P_n close to the unstable range, increasing the ratio of hot component and rising its temperature.

Temporal evolution of high- β plasma formation is shown in figure 3. The plasma was generated with applied microwave power of 20 kW at 2.45 GHz and 25 kW at 8.2 GHz both injected from $t = 0$ to 1 s at $P_n = 0.5 \text{ mPa}$. At this neutral gas pressure, there is a time lag between the start of microwave injection and high-density plasma formation. The time lag is lengthened and stable high- β discharge is difficult to sustain by decreasing P_n . (i) From $t = 0$ to 0.46 s , very low-density (typically $\sim 10^{15} \text{ m}^{-3}$) plasma was generated with strong x-ray radiation, suggesting thin plasma consists of extremely hot electrons. Microwave at 2.45 GHz was not effectively absorbed in this period. (ii) The reflection power gradually decreased during continuous microwave injection, and a jump to a high-density state was observed at $t = 0.46 \text{ s}$ accompanied with rapid increase in visible light strength. Then, the strength of visible light dropped rapidly and the stored energy started to increase. (iii) After the increase in stored energy saturated, the high- β stable state was realized. In the data shot presented in figure 3, the maximum local β was calculated to be 70% . The diamagnetic signals measured by

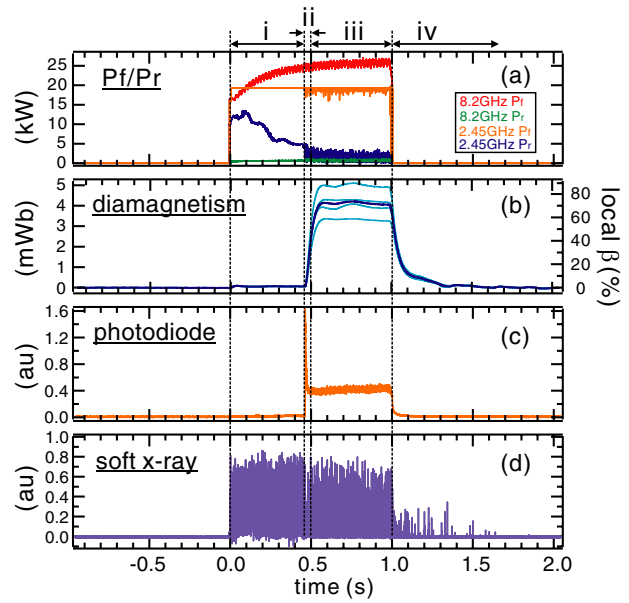


Figure 3. (a)–(d) Typical waveforms of high- β (local $\beta \sim 70\%$) plasma formation.

four magnetic loops were well reconstructed by an equilibrium calculation using a pressure profile peaked at $r = 49 \text{ cm}$ on the $z = 0 \text{ cm}$ plane. The plasma had a typical density of $1 \times 10^{17} \text{ m}^{-3}$ in this phase. (iv) After microwaves were turned off at $t = 1 \text{ s}$, plasma density and diamagnetic signal decayed slowly in the ‘afterglow’ phase.

Figure 4(a) shows the behaviours of magnetic fluctuations measured by a pickup coil in phase (i) of another discharge with similar conditions. After the onset of instability at $t = 105.6 \text{ ms}$, the lowest mode frequency ascended from 0.5 to 3 MHz . The chirping rate df/dt was correlated with conditions of plasma formation, and faster sweep was observed by increasing P_f and decreasing P_n . After $t = 112 \text{ ms}$, rapid growth and decay of fluctuation and frequency sweep were repeatedly observed. In this phase, the fluctuation amplitude tends to decay with saturation of frequency sweeping. These high-frequency modes are stabilized after the formation of high-density plasma and were not observed in phase (iii). Simultaneous measurements of the electron line density and fluctuation are shown in figure 5(a). When P_n is lower than approximately 0.4 mPa , however, rapid decrease in β and n_e , or plasma disruption, was sometimes observed during high-density state with the onset of instability. Figure 4(b) shows another low-frequency fluctuation mode measured by the 75 GHz interferometer. This fluctuation has a coherent mode structure, and its frequency tends to decrease with increasing n_e . The same fluctuation mode was also observed by a reflectometer, magnetic probes and Langmuir probes. The characteristics of the high- and low-frequency fluctuations are similar to electrostatic modes observed in LDX [19]. As shown in figure 5(b), emergence of the high-frequency fluctuation was observed only when P_n was low ($\lesssim 2 \text{ mPa}$) and a large amount of hot electrons was generated, suggesting that the effects of hot electrons are possible reasons for the onset of instability. Further investigation is needed to identify the observed fluctuation modes in RT-1.

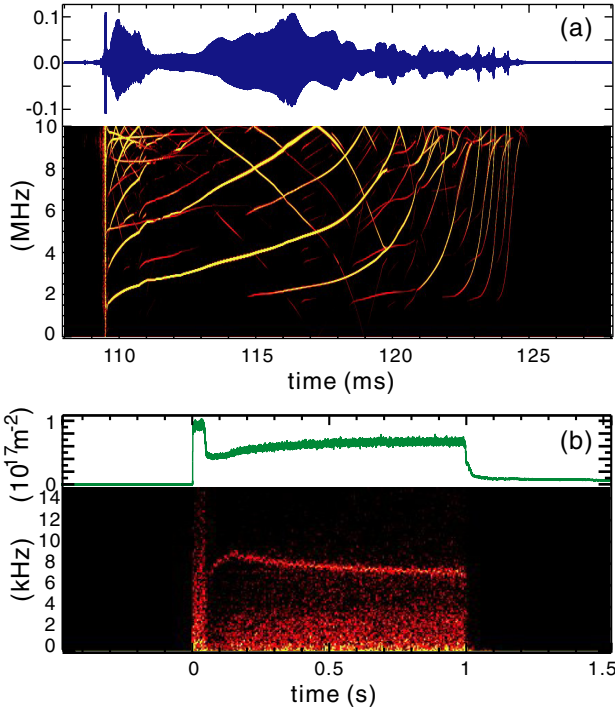


Figure 4. Fluctuations and its power spectrum (a) measured by a magnetic probe in low-density and extremely hot-electron mode (phase i of figure 3(a)) and (b) measured by an interferometer in a different condition.

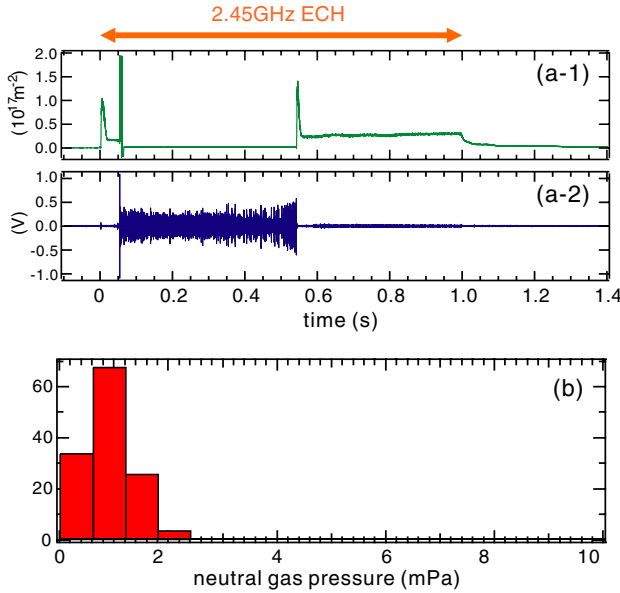


Figure 5. Behaviours of (a-1) electron line density and (a-2) electromagnetic fluctuation when neutral gas pressure $P_n = 0.8$ mPa. (b) Frequency counts of magnetic fluctuation emergence for various P_n ranging from 0.3 to 10 mPa.

4. Properties of hot electron plasma and confinement time

Figure 6(a) shows temperature T_h and density n_h of hot electrons measured by a Si(Li) detector located at the tangential port. Plasma was generated by injecting $P_f = 4$ kW of 2.45 GHz microwave at various P_n , neutral gas pressure. Experiment with the Si(Li) detector was conducted at relatively

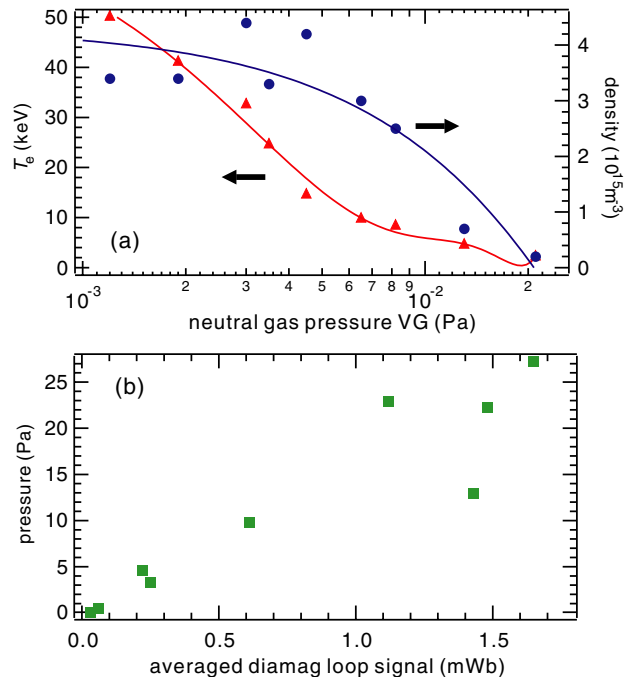


Figure 6. (a) Temperature T_h (triangles) and density n_h (circles) of hot electrons in the variation of filled neutral gas. (b) Hot electron pressure $P_h = n_h T_h$ in the variation of diamagnetic signal. 2.45 GHz microwave power was $P_f = 4$ kW and $n_e \sim 1 \times 10^{16} \text{ m}^{-3}$.

small P_f due to a problem of microwave noise on the detector. Assuming a Maxwellian energy distribution of hot electrons, bremsstrahlung photon number dN/dE_x due to interaction between free electrons and ions is proportional to $n_h n_i Z_{\text{eff}}^2 \exp(-E_x/T_h)/E_x T_h^{0.5}$, where Z_{eff} is the effective charge and E_x is photon energy [20]. T_h was estimated from PHA data of the detector by the curve fitting method to dN/dE_x including the effects of the transmittance of a Be window and photon efficiency of the Si(Li) detector. Then T_h was used to determine n_h , supposing that plasma consists of fully ionized hydrogen ions and taking plasma volume and detection angle into account. We note that the collision effects of electrons with neutral molecules may not be negligible for relatively low- β plasma, where the neutral gas density is comparable to that of plasma. By decreasing P_n , increase in T_h and n_h was observed. $P_h = n_h T_h$ was consistent with the diamagnetic measurements when hot electrons were major components of electrons. Strong correlation between P_h and diamagnetism (figure 6(b)) also indicates that plasma pressure mainly results from hot electrons in such cases.

There are two electron populations with different temperatures in the ECH plasma in RT-1, and the hot component has very long particle and energy confinement times. Soft x-ray measurements using Si(Li) detectors show that the hot-electron component is in the temperature range from 1 to 50 keV. Edge Langmuir probe measurements show that the plasma also has cold electrons around 10 eV. The hot-electron component has relatively long confinement time due to its small cross section of collisions with other particles. The decay curve of electron line density after the microwave was turned off and has two different time constants, corresponding to hot and cold components of electrons. Figure 7 shows the

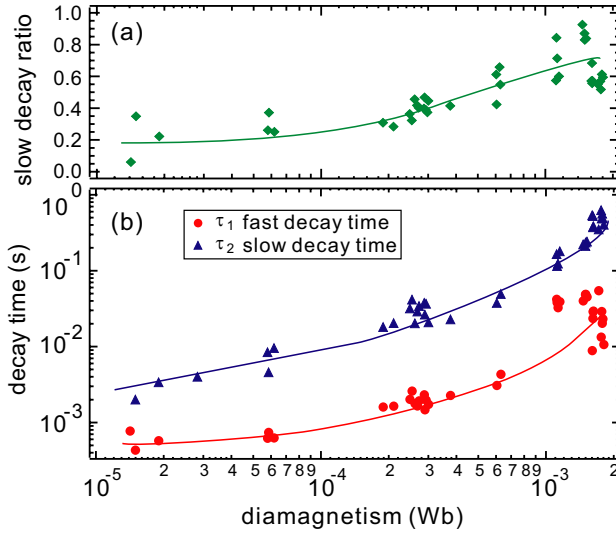


Figure 7. (a) Ratio of slow decay component electrons observed by interferometer and (b) decay time constants of fast and slow components at various neutral gas pressure.

ratio of slow decay density components, and the time constants of fast and slow decay measured by double exponential fitting of the decay curve. By optimizing neutral gas pressure, increases in the ratio of the hot component and in the decay time were observed. The maximum confinement time of plasma density was $\tau_p = 0.6$ s. Diamagnetic measurements showed that energy confinement time τ_e was comparable to τ_p . It suggests that temporal variation of T_h in the afterglow phase was relatively small, and is consistent with soft x-ray measurements in the afterglow phase. Using typical parameters $T_h = 50$ keV, $n_e = 10^{17} \text{ m}^{-3}$, $B = 0.1$ T in the core region, and plasma radius $r_p = 0.3$ m, the Bohm diffusion time and the classical diffusion time are calculated to be $\tau_B \sim 1.4 \mu\text{s}$ and $\tau_c = 3.0 \times 10^3$ s, and we have $\tau_p \sim 4 \times 10^5 \tau_B$ and $\tau_p \sim 2 \times 10^{-4} \tau_c$.

5. Peaked density profiles and inward diffusion of particles

Radial density profiles of the plasma were estimated from multichord measurements of the 75 GHz interferometer. Because the interferometer has only 1 ch, simultaneous multichord measurements were not carried out at present. Electron line density n_l was repeatedly measured at three different chords in similar plasma formation conditions with good reproducibility. The horn antennas of the interferometer were set at tangential ports at $y = 45$ cm (chord 1) or vertical ports at $r = 62$ cm (chord 2) or $r = 72$ cm (chord 3). The light path of the tangential chord is close to the dipole field coil, while those of vertical ports are rather close to the chamber wall (figure 1). We assume that the electron density is a function of the magnetic surface $\Psi = rA_\theta$ and has power-law dependence on r , on the equator ($z = 0$ cm) plane of the chamber,

$$n(r) = n_0 r^{-a}. \quad (1)$$

Then we can calculate n_0 and a , and estimate the radial density profile of plasma using interferometer data obtained at two chords.

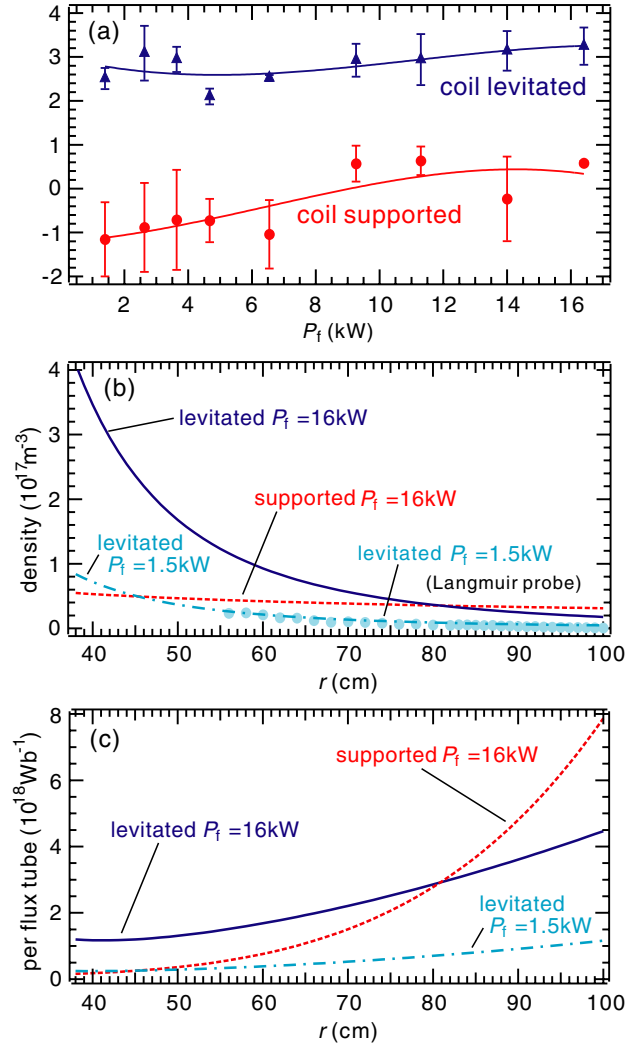


Figure 8. (a) Coefficient a of equation (1) with and without coil levitation at various 2.45 GHz microwave power. (b) Radial electron density profiles inferred from measurements of the interferometer. Measurements with a Langmuir probe are also shown for comparison for small P_f . (c) Radial profiles of particle numbers per flux tube.

Figure 8(a) shows a in (1) for various P_f of 2.45 GHz microwave with and without coil levitation. Using the line density data measured at chords 1 and 2, and chords 1 and 3, we calculated two sets of n_0 and a values. The data plotted in the figure show the averaged values of the calculated a . The error bars show the variations of a for the two sets of measurements. When the magnet was not levitated, the dipole field coil was operated at 90% of its rated current, so that the shapes of the magnetic surfaces in both cases were quite similar. Thus, variation in plasma properties is attributed solely to the effects of the coil support structure. By coil levitation, a drastic increase in n_l was observed in the measurement at the tangential chord, indicating the increase in n_e in a strong field region. As shown in figure 8(a), $a = -0.3 \pm 0.7$ when the coil was not levitated, and $a = 2.8 \pm 0.4$ when levitated. The solid and dotted lines in figure 8(b) show the estimated n_e profiles when $P_f = 16$ kW with and without coil levitation. By removing perturbations due to the coil support structure, peaked density profile is realized [4]. When P_f is small,

an edge Langmuir probe can be used for the measurement of radial n_e profiles. The chain line in figure 8(b) show n_e profiles measured by the interferometer when $P_f = 1.5$ kW with coil levitation, which shows good agreement with that of the Langmuir probe at the edge region, plotted as closed circles in the figure. It indicates that the estimation of density profiles using the interferometer is consistent with the local measurements with the Langmuir probe. Figure 8(c) shows the electron numbers of plasma per flux tube, showing that the density per flux tube rather flattens when the coil was levitated.

These observations are consistent with the self-organization of the peaked density profile of plasma in the magnetospheric configuration. The plasma profile does not strongly depend on formation conditions (figure 8(a)) other than the effects of strongly disturbing coil support structures. We note that peaked density profiles of charged particles in the magnetospheric configuration were also observed in experiments with pure electron plasma. In RT-1, toroidal non-neutral plasma consisting of only electrons is stably trapped for more than 300 s [3, 21, 22]. The electron plasma has a large electrostatic fluctuation in the diocotron (Kelvin–Helmholtz) [23] frequency range during beam injection, which can cause radial penetration of electrons breaking conservation of the third adiabatic invariant. Inward pinch of charged particles in a magnetospheric configuration was theoretically predicted by Hasegawa [1, 2]. He pointed out that plasma satisfies $\partial f / \partial \Psi = 0$ in a stable equilibrium state, where there is no driving force of drift wave turbulence. Here $f(\mu, J, \Psi)$ is the phase space density as a function of the adiabatic invariants, and turbulent-induced diffusion occurs until the plasma density per flux tube becomes constant. In the strongly inhomogeneous dipole field, the stable condition requires strongly peaked density profiles in the strong field region. Observation of the density flattening in the phase space and self-organization of stable vortex structures [3, 4] are consistent with the predicted turbulent-induced inward diffusion, and is one of the fundamental mechanisms of the relaxation process of plasma in the magnetospheric configuration.

6. Summary

In this study, we reported the experimental results on high- β plasma in RT-1 mainly based on the measurements with interferometer and x-ray detectors. By the effects of improved geomagnetic-field compensation, optimized neutral gas pressure, and increased microwave powers, the local β of plasma has reached 70%, with corresponding diamagnetic loop signal of 4.2 mWb. Low-density plasma has electromagnetic fluctuations, which sometimes cause serious instability, but they were stabilized by optimizing the neutral gas pressure, resulting in a stable high- β state. The results of diamagnetic measurements with Grad–Shafranov analysis are consistent with x-ray measurements. It is estimated that the main component of the hot plasma is high-temperature electrons with ~ 50 keV, and its confinement time is ~ 0.5 s. Multi-chord interferometer measurements showed that the plasma has strongly peaked density profiles in the strong field region. This observation is consistent with previously reported results with pure electron plasma, and agrees with

the theoretically predicted ‘flattening’ of charged particles in magnetic coordinates.

Acknowledgments

This work was supported by Grants-in-Aid for Scientific Research (14102033 and 19340170) from MEXT of Japan.

References

- [1] Hasegawa A. 1987 A dipole field fusion reactor *Comment. Plasma Phys. Controlled Fusion* **11** 147
- [2] Hasegawa A., Chen L. and Mauel M.E. 1990 A D-³He fusion reactor based on a dipole magnetic field *Nucl. Fusion* **30** 2405
- [3] Yoshida Z. *et al* 2010 Magnetospheric vortex formation: self-organized confinement of charged particles *Phys. Rev. Lett.* **104** 235004
- [4] Boxer A.C. *et al* 2010 Turbulent inward pinch of plasma confined by a levitated dipole magnet *Nature Phys.* **6** 207
- [5] Krimigis S.M. *et al* 1979 Hot plasma environment at Jupiter: Voyager 2 results *Science* **206** 977
- [6] Mahajan S.M. and Yoshida Z. 1998 Double curl Beltrami flow: diamagnetic structures *Phys. Rev. Lett.* **81** 4863
- [7] Yoshida Z. and Mahajan S.M. 2002 Variational principles and self-organization in two-fluid plasmas *Phys. Rev. Lett.* **88** 095001
- [8] Shiraishi J. *et al* 2005 Relaxation of a quasisymmetric rotating plasma: a model of Jupiter’s magnetosphere *Phys. Plasmas* **12** 092901
- [9] Yoshida Z. *et al* 2010 Generalized two-fluid equilibria: understanding RT-1 experiments and beyond *Phys. Plasmas* **17** 112507
- [10] Yoshida Z. *et al* 2006 First plasma in the RT-1 device *Plasma Fusion Res.* **1** 008
- [11] Yoshida Z. *et al* 2007 RT-1 project: magnetosphere-like plasma experiment *Fusion Sci. Technol.* **51** 29
- [12] Morikawa J. *et al* 2007 Development of a super-conducting levitated coil system in the RT-1 magnetospheric configuration device *Fusion Eng. Des.* **82** 1437
- [13] Ogawa Y. *et al* 2008 Construction and operation of an internal coil device, RT-1, with a high-temperature superconductor *Plasma Fusion Res.* **4** 020
- [14] Yano Y. *et al* 2010 Feedback control of the position of the levitated superconducting magnet in the RT-1 device *Fusion Eng. Des.* **85** 641
- [15] Yano Y. *et al* 2009 Improvement of field accuracy and plasma performance in the RT-1 device *Plasma Fusion Res.* **4** 039
- [16] Kobayashi S., Rogers B.N. and Dorland W. 2010 Particle pinch in gyrokinetic simulations of closed field-line systems *Phys. Rev. Lett.* **105** 235004
- [17] Bourdelle C. 2005 Turbulent particle transport in magnetized fusion plasma *Plasma Phys. Control. Fusion* **47** A317
- [18] Saitoh H. *et al* 2009 Initial results of x-ray imaging and energy spectrum measurements of hot electron plasmas in RT-1 *Plasma Fusion Res.* **4** 050
- [19] Garnier D.T. *et al* 2006 Production and study of high-beta plasma confined by a superconducting dipole magnet *Phys. Plasmas* **13** 056111
- [20] Hutchinson I.H. 2002 *Principles of Plasma Diagnostics* (Cambridge: Cambridge University Press)
- [21] Saitoh H. *et al* 2009 Measurement of the density profile of a toroidal non-neutral plasma by a wall-probe array *Plasma Fusion Res.* **4** 054
- [22] Saitoh H. *et al* 2010 Confinement of electron plasma by levitating dipole magnet *Phys. Plasmas* **17** 112111
- [23] Levy R.H. *et al* 1969 Ion resonance instability in grossly nonneutral plasmas *Phys. Fluids* **12** 2616